



# Mechanical properties and corrosion resistance of hot extruded Mg–2.5Zn–1Ca alloy



Dexue Liu <sup>a,b,\*</sup>, Chenggong Guo <sup>a</sup>, Liqiang Chai <sup>a</sup>, Vincent R. Sherman <sup>b</sup>, Xiaoqiong Qin <sup>a</sup>, Yutian Ding <sup>a</sup>, Marc A. Meyers <sup>b</sup>

<sup>a</sup> State Key Laboratory of Advanced Processing and Recycling of Non-Ferrous Metals, Lanzhou University of Technology, Lanzhou 730050, China

<sup>b</sup> Department of Mechanical and Aerospace Engineering, University of California, San Diego, CA 92093-0411, USA

## ARTICLE INFO

### Article history:

Received 14 August 2014

Received in revised form 27 January 2015

Accepted 2 February 2015

Available online 14 February 2015

### Keywords:

Magnesium alloy

Processing routes

Hot extrusion

Fine grain strengthening

Corrosion resistance

## ABSTRACT

It is demonstrated that the mechanical properties and corrosion resistance of Mg–2.5 wt%Zn–1 wt%Ca alloy are enhanced by the microstructural changes imparted by hot extrusion. A processing procedure is developed to form hollow tubes with an outer diameter of ~2.0 mm and wall thickness of ~0.1 mm, which is well suited for subsequent stent manufacturing. The influence of thermal and mechanical processing on corrosion and plasticity was found to be associated with grain-size reduction and the redistribution of intermetallic particles within the microstructure, providing significant improvement of performance over the cast alloy. Observation of the fracture surfaces reveals a mode transition from brittle (cast) to ductile (processed). Enhanced mechanical properties and decreased resorption rate represent significantly improved performance of this alloy after the novel processing sequence. Based on the improved properties, the produced Mg alloy is more suitable for practical *in vivo* applications.

© 2015 Elsevier B.V. All rights reserved.

## 1. Introduction

Biodegradable implants with satisfactory mechanical properties provide significant advantages in certain applications, as the requirement for a second surgical procedure for removal is eliminated. Early use of magnesium alloys as a resorbable biomaterial dates from the 1930s [1,2]. One problem commonly encountered is that the rapid corrosion experienced in the body, leading to the accumulation of subcutaneous gas bubbles [3]. The interest in magnesium alloys has been reactivated as new compositions with much lower dissolution rates have been developed.

Degradable magnesium alloys have significant advantages over biodegradable polymers and ceramics as potential biomaterials due to their appropriate mechanical properties and excellent biocompatibility, especially in cardiovascular disease treatment [4,5]. Conventional implant stents typically use corrosion resistant metals such as stainless steels, Ti, Co, and Cr based alloys. The stents remain in the body permanently even when they are no longer needed [6,7]. Biodegradable polymers and ceramic-based

composites, although promising, but they may not provide sufficient strength, ductility, or biocompatibility for orthopedic applications [8,9]. It is therefore essential for an orthopedic biodegradable implant to have a degradation rate that matches the healing or regeneration process of blood vessels.

The advantages of Mg alloys over other biomaterials as a replacement of permanent vascular implants have attracted considerable attention [10]. However, both *in vitro* and *in vivo* evaluations of the current Mg alloys show that they degrade much faster than desired [11,12]. Therefore, there is of great interest to enhance the mechanical properties and reduce the corrosion rate to satisfy the requirements of cardiovascular disease treatment in biological stress environment [13]. Magnesium alloys are difficult to deform because of the poor ductility caused by their hexagonal structure and limited slip systems. Thus, it is necessary to develop processes that can simultaneously enhance the plasticity and control the rate of biodegradation.

Numerous studies have addressed separately the mechanical or corrosion properties, while none of them considered the influence of processes on both performance aspects of implant stents. It is desirable to maintain the required mechanical strength of Mg alloy implant stent when it degrades at a prescribed rate. From the corrosion perspective, different surface modification techniques have been used for improving corrosion resistance [14–16]. However, the rate of degradation increases sharply once the specially treated surface is dissolved [17–19]. For most metals, improvements

\* Corresponding author at: State Key Laboratory of Advanced Processing and Recycling of Non-Ferrous Metals, School of Material Science and Engineering, Lanzhou University of Technology, Langongping Road 287, Lanzhou City, Gansu Province 730050, China. Tel.: +86 13919947009; fax: +86 931 2976702.

E-mail address: [dexeliu@hotmail.com](mailto:dexeliu@hotmail.com) (D. Liu).

in mechanical properties and corrosion resistance can also be effectively achieved through alloying and processing [20,21]. In addition, for medical Mg alloys, the biocompatibility of many alloying elements is limited [22–24]. Moreover, most of the research on biodegradable Mg alloys focused on original alloys, ignoring the dynamic response when it is processed from one state to another. Some processing steps are necessary for the manufacture of the implant stent when it is transformed from the original alloy to the desired geometrical shape. Thus, the properties of alloys are inevitably altered in this process [25]. Based on the complicated processing routines for a precise micro-tube, the difference between processed samples and original ones are explored in this work.

Ca and Zn elements are reported to have good biocompatibility [19,23,26]. The mechanical and corrosion properties of cast Mg–Zn–Ca with different compositions have been extensively investigated as the most promising biodegradable materials. It is also reported that yield strength of Mg alloys increased with RE additions, corrosion rates also systematically increased, however, this depended on the type of RE element added and the combination of elements added [27]. In this paper, based on design of alloy composition, we introduced a typical processing sequence required for forming Mg–Zn–Ca alloy tubes with ~2 mm outer diameter and ~0.1 mm wall thickness. There is a high demand of these micro-tubes for stent applications. The optimum design of alloy composition, vacuum melting, heat-treatment, integrated plastic deformation and micro-tube forward extrusion are included in the processing technique. Significant improvements in mechanical properties and better corrosion resistance were achieved through this processing sequence. This work aims to determine whether the grain size or plastic deformation during the forming processes of implant stent are the predominant factors controlling the degradation response, and to what extent the mechanical properties and corrosion resistance of Mg–2.5Zn–1Ca alloy can be altered simultaneously by the processes imparted, when taking into account that both of them would influence each other during the degradation process for a implant stent.

## 2. Experimental procedures

### 2.1. Preparation of materials and heat-treatment

The composition of the experimental alloy was Mg–2.5 wt %Zn–1 wt%Ca. Commercially pure Mg (99.99 wt%), Zn (99.99 wt%) and Mg–10 wt%Ca intermediate alloy powders were melted and cast in vacuum induction melting furnace (Institute of Vacuum Technology, Shenyang, China) in a high purity argon atmosphere. Differential scanning calorimetry (DSC) was performed (Netzsch – 400, Germany) at constant heating and cooling rates of 10 K/min between 20 and 600 °C to evaluate the thermal properties of the cast samples. The results of analysis were used for selecting the temperature for heat-treatment and subsequent plastic deformation. The cast ingots were subjected to solution heat-treatment and homogenizing annealing. The solution heat-treatment temperatures were 390 ± 5 °C, 410 ± 5 °C and 430 ± 5 °C; the holding time was 24 h. The annealing temperatures were 390 ± 5 °C, 400 ± 5 °C and 410 ± 5 °C; the holding time was also 24 h. All treated samples were ultrasonically cleaned in distilled water and dried in air before further characterization.

### 2.2. Hot extrusion

A cast ingot was machined into cylinders with a diameter of 72 mm after the oxide skin was removed. The extrusion equipment was a 3150 kN hydraulic pressure machine (Tianduan Press Co. Ltd.

China). The extrusion die temperature was set at 300 ± 5 °C, and the sample was heated in a muffle furnace (SRJX-4-13, Shanghai Zhongheng Instrument Co. Ltd. China) prior to extrusion. The extrusion speed was set at 4 mm/s. The extruded rod diameter is 12 mm, representing an extrusion ratio of 36:1. The extruded rods were machined into tubular billets with outer diameter of 10 mm and inner diameter of 3 mm. These tubular billets were subjected to conventional tube extrusion at 360 ± 5 °C. The sample was put in the die and the two were heated together to ensure an accurate pressing temperature. Tubes with outer diameter of 3.0 mm and wall thickness less than 0.16 mm were obtained; this is close to the desired size of micro-tubes for stent implants. Further processing steps are needed to manufacture microtubes with precise size. These steps include slight drawing, straightening and polishing, which have negligible influence on the properties of material. Eventually, we got a micro-tube with outer diameter of ~2.0 mm that satisfied for an implant stent manufacture.

### 2.3. Microstructural characterization

First, the cast and extruded samples were polished and etched with a mixture of 2 ml of acetic acid (36%), 2 ml of nitric acid (68%), and 196 ml of water. Microstructures of all the samples were then observed in a MeF3 optical microscope (Reickert-Jung Co. Austria) after mechanical polishing and etching with Nital. Scanning electron microscope (JSM-5600LV, JEOL Ltd. Japan)-energy dispersive spectrometer (Kevex-7000, USA) (SEM-EDS) analysis was performed to investigate the elemental distribution. X-ray diffractometry (D/max- $\gamma$ B rotating anode XRD, Rigaku Co. Japan) using Cu  $K_{\alpha}$  radiation was employed for the identification of the constituent phases in the cast, heat-treated, and extruded samples.

### 2.4. Mechanical testing

Standard surface-smooth tensile samples were machined according to American Society of Testing Materials (ASTM) international standards E8M-93. The length and cross-sectional diameter of the specimens were 17 mm and 4 mm respectively. The tensile tests were carried out in a universal material testing machine (AG-10TA, Shimadzu Co. Japan) with a strain rate of 0.05 mm/s, at 20 °C. To control the precision, 3 samples were tested as a group for each tensile test. Tensile strengths, yield strengths and elongations of Mg–2.5Zn–1Ca were established from the stress–strain curves.

### 2.5. Corrosion testing

The preparation, cleaning, and evaluation of corrosion testing were carried out according to ASTM G1-1999; the immersion test was conducted according to ASTM G31-72 (2004) in Hank's solution, one of the most commonly used balanced salt solutions in biomedical experiments. The cylindrical corrosion test sample size is 20 mm diameter and 3 mm height. In particular, because of the relative bulk of the micro-tube, immersion test was conducted with a surrogate sample processed according to the same methodology, maintaining the same extrusion ratio. Experimental samples were immersed in a 50 ml solution for 8 days at a temperature of 37 °C. Three samples were tested in parallel for each group. The samples were removed from Hank's Balanced Salt Solution, rinsed with distilled water, dried at room temperature, and subsequently ultrasonically cleaned in a solution of 200 g/L CrO<sub>3</sub> + 10 g/L AgNO<sub>3</sub> (Sinopharm Chemical Reagent Co. Ltd. China) at room temperature for 10 min. Corrosion resistance variation of samples was monitored by the pH value of the corrosion media. The corrosion weight loss rate was used for calculating the average corrosion

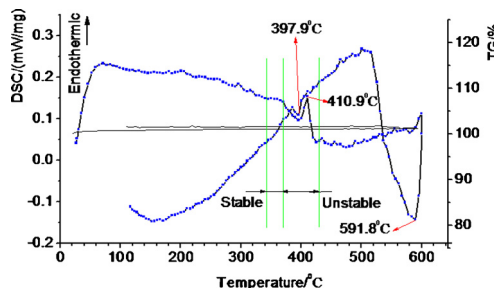


**Fig. 1.** DSC curves for the cast alloy at constant heating and cooling rates of 10 K/min.

rate. Corrosion morphologies of Mg alloy after immersion in Hank's solution for 8 days were characterized by SEM.

## 2.6. Statistical analysis

To investigate the results of mechanical and immersion test, Student's *t*-test of significance was executed by SPSS (statistical product and service solutions) 13.0 for statistical analysis. The test is applied to analyze the significance of difference between two average values, when the sample size is under 30. T distribution theory is used to infer differences in the probability of occurrence, thereby determining whether the differences of the two are meaningful.

## 3. Experimental results

### 3.1. Processing temperature

Cast samples were tested by DSC to establish their potential phase transitions and processing temperatures, as shown in Fig. 1. Both heating and cooling curves show that there are no obvious endothermic or exothermic peaks from 340 to 370 °C. Reactions are observed between 390 and 420 °C, and are marked in Fig. 1. Therefore, taking into account poor ductility due to thermal loss and possible grain growth due to overheating, hot extrusion was conducted at approximately 360 °C to keep material deformation at a stable microstructural state. The subsequent heat-treatment procedures were conducted within this temperature range for this reason.

### 3.2. Microstructure evolution

The evolution of the distribution of intermetallic particles and the compositional distribution imparted by processing are illustrated in Fig. 2. Fig. 2(a) illustrates the initial structure, characterized by a large average grain size of ~180 μm. The cast alloy is composed of large irregular cellular grains; there is some precipitation along grain boundaries, which is distributed in spotty or intermittent shapes. The microstructure characteristic of large grains leads to poor plasticity. As shown in Figs. 3(a) and 4, the X-ray diffraction spectrum as well as EDS results indicate that the alloy is mainly composed of α-Mg phase and Ca<sub>2</sub>Mg<sub>6</sub>Zn<sub>3</sub> intermetallic, present as a precipitate. Fig. 2(b) shows the grain structure of the alloy processed by homogenizing annealing and solution treatment. The microstructure tends to be uniform and dendritic segregation is reduced or eliminated. Fig. 5(a) shows the back-scattering topography for samples after a series of heat treatment. White spots dispersed in matrix and along the grain boundary represent the precipitates we mentioned above. Element contents of those precipitates were tested by EDS and the results indicated that composition of them are still Ca<sub>2</sub>Mg<sub>6</sub>Zn<sub>3</sub> intermetallic. Fig. 2(c) shows the grain structure of the alloy extruded with a ratio of 36:1

and Fig. 2(d) shows the grain structure of the alloy extruded to a micro-tube based on the extruded rod. The eutectic structure in grain boundaries broke down and dissolved into the alpha-Mg matrix. The foregoing illustrated Ca<sub>2</sub>Mg<sub>6</sub>Zn<sub>3</sub> phase was not detected by XRD, as shown in Fig. 3(b), however, traces of it was detected by back-scattering test, as shown in Fig. 5(b). It means that remarkable grain refinement took place along with precipitate fragmentation. The extruded alloy is composed of smaller and comparatively regular grains. The cellular grains disappear and large numbers of fine equiaxed grains appear. A small amount of dendrites can also be observed. The average grain size of the extruded rod is ~26 μm. This grain size is reduced to 10 μm for the microtube extrusion.

The distribution of intermetallic particles in cast alloys is illustrated in the SEM micrograph and EDS images in Fig. 4. Fig. 4(a) shows 2–3 μm granular precipitates distributed in the matrix and bands of precipitates distributed along the grain boundary. Fig. 4(b) indicates that the weight percentage of Zn (1.20 wt%) and Ca (0.44 wt%) are lower than the original alloying composition. This is likely due to the low solid solubility of Zn and Ca in the Mg matrix. As shown in Fig. 4(c) and (d), the mole fractions of Mg, Zn and Ca in granular precipitation are 73.20%, 16.24% and 10.56% respectively; the corresponding values in the grain-boundary precipitation bands are 94.32%, 3.51% and 2.17%. EDS data analysis revealed that the atomic ratio for Ca:Zn is about 2:3 both in granular and band precipitates. One can establish that the precipitates are Ca<sub>2</sub>Mg<sub>6</sub>Zn<sub>3</sub> [26], which could also be verified by XRD results, as shown in Fig. 3(a).

### 3.3. Mechanical characterization

The addition of Zn is known to strengthen Mg alloys. However, it can also reduce the corrosion resistance when it is higher than 2.5%. It may also have potential toxic influence on the biological environment [28]. Therefore, the Zn content was fixed at 2.5 wt%. The addition of Ca was adopted because of its excellent biocompatibility and potential to influence the mechanical properties. Fig. 6(a) shows the mechanical properties of specimens with Ca content ranging from 0.3 wt% to 1.5 wt%. It is clear from Fig. 6(a) that the alloy has the highest yield strength and elongation when the Ca content is 1 wt%. Therefore, a Mg alloy with a nominal composition Mg–2.5Zn–1Ca (wt%) was selected for further investigation because of its higher yield strength and elongation. The mechanical properties were evaluated by tensile tests at room temperature following four processing procedures. The yield and tensile strengths of original alloy are 125 and 216 MPa, respectively, with 15% tensile elongation. Fig. 6(b) shows that the overall mechanical properties of specimens improve significantly after processing. The tensile strength of specimen increased from 216 MPa to 309 MPa after it was processed with heat-treatment and hot extrusion. The yield strength also increased from 125 MPa to 192 MPa. The extruded rod has improved ductility, as its elongation increased significantly from its initial value of 15–34%. It is very important for the samples to achieve better ductility through processing to satisfy the demands of a precision implant stent. The relative standard deviation (RSD) values for the extruded rod are as high as 20.9%, implying that samples with a high extrusion ratio are not homogeneous. The Young's moduli of cast alloy and extruded rod are 41.4 GPa and 42.9 GPa respectively, which is of the same order as the reported value of 20 GPa for human bone [29].

Student's *t*-test of significance was applied to do statistical analysis. The results indicated that there are no significant differences among most of the values for samples with different Ca content, as shown in Fig. 6(a). However, there are significant differences among most values for samples produced by the processing procedures mentioned above, as shown in Fig. 6(b). This significance shows

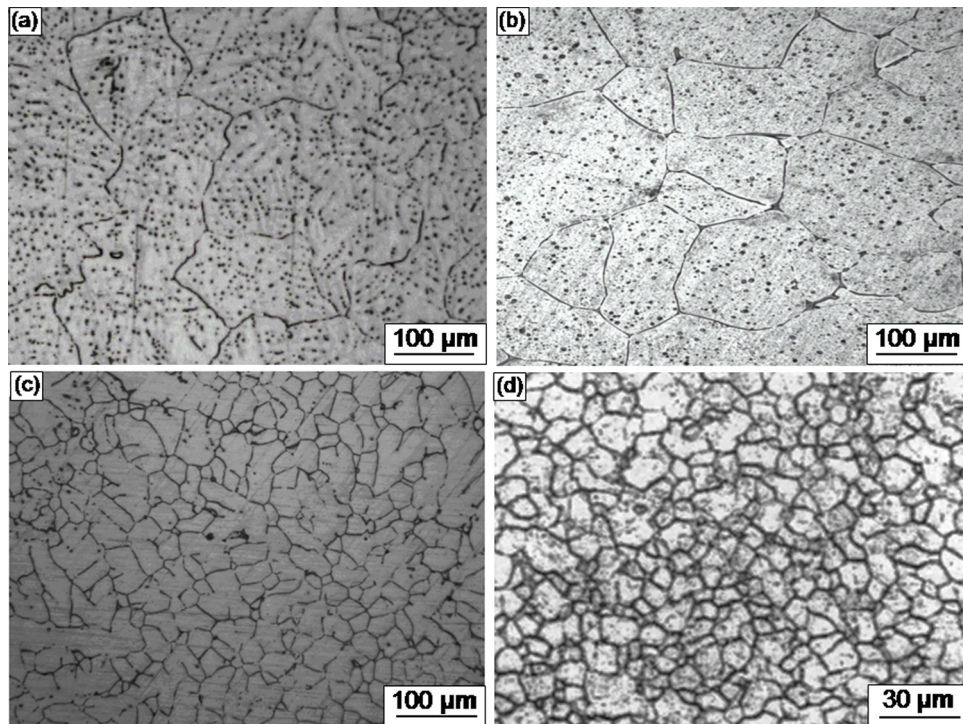


**Fig. 2.** Mechanical properties (yield strength, tensile strength and elongation) of different specimens: (a) Mg–2.5Zn–xCa with different Ca contents ranging from 0.3 wt% to 1.5 wt%; (b) Mg–2.5Zn–1Ca tested in different conditions.

that the procedures are effective to improve the alloy's mechanical properties.

#### 3.4. Tensile fracture surface

The evolution of the tensile fracture surface as a function of processing is presented in the SEM fractographs in Fig. 7. Fig. 7(a) shows the morphology of the tensile fracture surface for the cast sample. Cleavage planes and tearing ridges, which are typical of brittle fracture, can be seen on the tensile fracture surfaces of the cast alloy. It is a mixed type with cleavage fracture, quasi-cleavage fracture and intergranular fracture. As shown in Fig. 7(b), the heat-treated condition has a fracture composed of cleavage planes, tearing ridges and dimples. This observation implies that the heat-treated sample shows mixed ductile and brittle fracture features. Fig. 7(c) presents the extruded rod with an extrusion ratio of 36:1. Fracture features indicative of improved toughness can be observed. The tearing ridge and a large amount of dimples with different sizes are clear. Dispersed cleavage steps imply that the fracture mode of the alloy is based mainly on quasi-cleavage ductile fracture. Fig. 7(d) presents the tensile fracture surface of extruded micro-tube. It is entirely composed of dimples with varying sizes, indicative of significant plastic deformation prior to failure.

#### 3.5. Corrosion resistance with grain refinement

Fig. 8(a) displayed the corrosion rate of samples immersed in Hank's solution for 8 days, and the results of the first 7 days were analyzed. The average corrosion rate was calculated based on the corrosion weight loss rate. It is observed that the corrosion rate of cast alloy tends to have large fluctuations. This unpredictability may be attributed to microstructural defects. The corrosion rate was not significantly improved by heat-treatment, but the structural homogeneity caused by the heat treatment eliminated the rate fluctuations experienced by the cast alloy. The lower

corrosion rates experienced by the extruded alloys indicate that hot extrusion has an influence on corrosion properties. The RSD of corrosion rate for cast alloy are much larger than that of alloys processed according to the methodology above. Intrinsic factors such as microstructure and solution influence and extrinsic factors such as immersion period, experimental error and calculation error influence the statistical results.

The corresponding pH value variation is presented in Fig. 8(b). It can be seen that pH values of solutions clearly decreased after double extrusion was performed on the alloy; they are shifted toward a neutral value of 7. That shows clearly that the microstructure evolution caused by solid solution strengthening and fine grain strengthening influence the corrosion properties of the alloy. The RSD of pH value for all the samples are smaller than 2.0%, indicating that the pH value variation curves are convinced for the immersion tests.

Student's *t*-test of significance was also performed to provide statistical analysis for the 4 groups of values for corrosion rate and pH value. Although there were no significant differences between cast alloys and heat treated alloys, as well as rod and tube, there were significant differences for most of the values between cast alloys and extruded alloys ( $P < 0.01$ ). This suggests that the processing procedures do enhance the Mg alloys' corrosion properties.

Fig. 9 shows the corrosion surface morphologies of cast alloy with heat-treatment and extruded micro-tube immersed in Hank's solution for 8 days. It can be seen that the cast alloy shows severe non-uniform corrosion features. A number of large corrosion pits with varying depths can be seen in the surface of the specimen. In contrast, the corrosion surface of the extruded micro-tube exhibits more even and planar features with a large concentration and uniform distribution of small corrosion pits. This explains why the Mg alloy processed by hot extrusion shows a reduced corrosion rate. The introduction of impurities and alloying elements to a Mg alloy leads to galvanic corrosion. Corrosion damage in a biologically representative solution of the

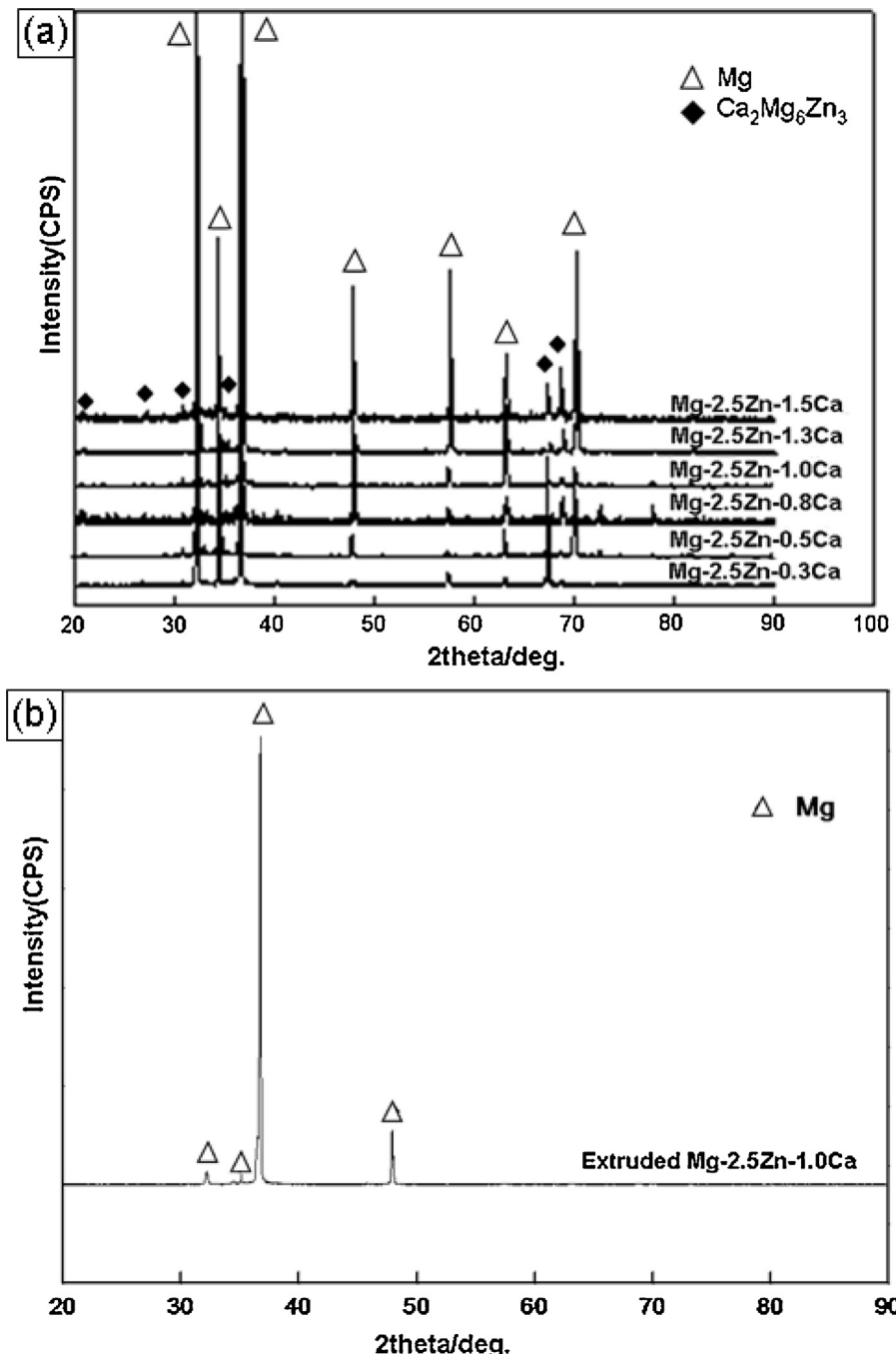


**Fig. 3.** SEM micrographs of: (a) as-cast Mg–2.5Zn–1Ca alloy; (b) EDS spectrum of area b in (a); (c) EDS spectrum of area c in (a); (d) EDS spectrum of area d in (a).

corrosion product film in the solution containing chlorine-ion is based on a pitting mechanism. The enhanced corrosion resistance of extruded Mg alloy indicates that the properties of surface passivation film can be improved by grain refinement.

#### 4. Discussion

It is apparent from Fig. 6 that the best overall mechanical properties were obtained in the Mg–2.5 wt%Zn–1 wt%Ca after heat-treatment and hot extrusion. The enhanced yield and tensile strengths satisfy the mechanical requirements of implant stents working in a biological environment. On the one hand, mechanical properties could have significant influence on degradation as demonstrated above. An implant stent would benefit from the

higher material strength to match the healing and regenerative processes. On the other hand, further processing procedures would profit from the enhanced elongation [30,31]. Both heat-treatment and hot extrusion improve the properties toward the requirements for stents. Mechanical properties are crucial for the stent to maintain mechanical integrity as it degrades in a biological environment.

Changes in mechanical properties have been previously reported for extruded Mg alloys with different extrusion rates and temperatures. Most of the results show increased mechanical properties, while some other results indicate a slight strength decrease in favor of increased elongation [32]. The thermal stability of the microstructure is an important factor for processing at appropriate temperatures. In this work, the hot extrusion temperature is slightly higher than  $\sim 0.5 T_m$  [31], where  $T_m$  is the absolute

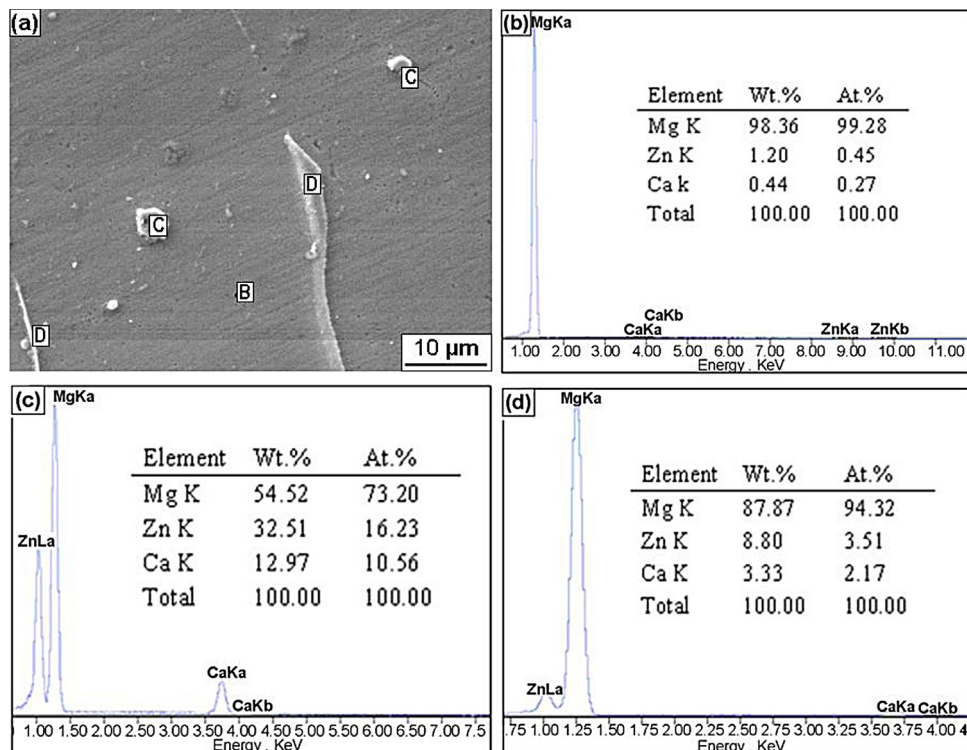


**Fig. 4.** X-ray diffraction patterns of: (a) cast alloys with different Ca contents ranging from 0.3 wt% to 1.5 wt%; (b) alloy processed by heat-treatment and hot extrusion.

melting temperature. It must be less than the temperature at which the grains grow, which is determined by the endothermic peak in the DSC test to be 411 °C. DSC heating-cooling curves also provide essential information on the phase transition characteristics as phase transition is usually an endothermic or exothermic processes [33]. Without precise temperature and strain rate control, it is difficult to enhance the elongation and strength.

Processing routes and the phase transition play an important role in processing procedures. The addition of Zn provides a relatively good solid solution strengthening effect since its solid solubility is 6.2 wt% [34]. The enhancement of mechanical properties can be attributed to both the solution strengthening and fine-grain strengthening resulting from the processing sequence applied to these alloys. The grain-size strengthening as a result of hot extrusion plays a critical role in increases in yield strength, which can be explained partially by the Hall-Petch equation:

$$\sigma_y = \sigma_0 + kd^{-1/2}$$

where  $k$  is the Hall-Petch slope, which has been reported within the range of 5–10 MPa mm<sup>1/2</sup> [35]. For the high-strength magnesium alloys, the reported value for the Hall-Petch coefficient lies in the range 280–320 MPa μm<sup>1/2</sup> [36]. Using a value of 300 MPa μm<sup>1/2</sup> we determine of  $\sigma_0$  for a grain size of 180 μm and yield stress of 125 MPa: 103 MPa. Using this  $\sigma_0$  value and a grain size of 26 μm, corresponding to the grain size as after double extrusion, a yield strength of 162 MPa can be estimated. The yield stress experimentally measured is higher: 192 MPa. That means not only fine grain strengthening but solid solution strengthening as well as other strengthening achieved through the whole procedures. Nevertheless, the above calculation illustrates the Hall-Petch grain size effect only on the yield stress.

The larger elongation obtained for the grain size of 10 μm can be explained in terms of the superplastic effect. Although the effect requires higher temperature and lower strain rates to reach its maximum potential [37], the increased ductility can be attributed to grain-boundary sliding, which increases in significance as the grain size is decreased.

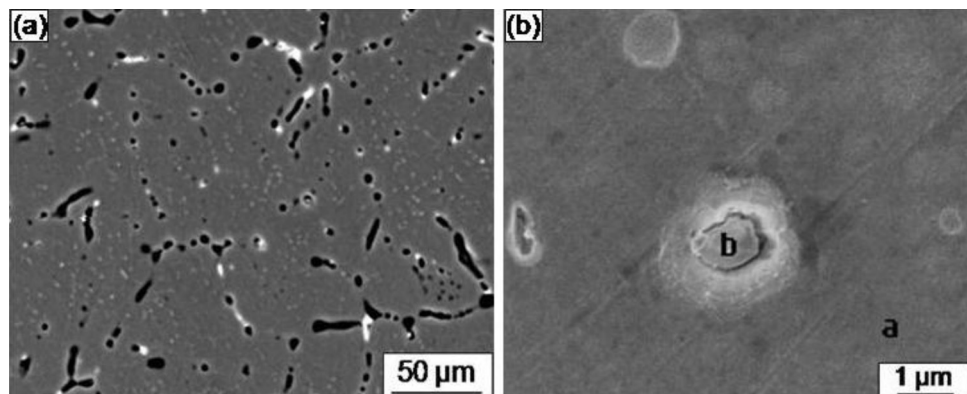


**Fig. 5.** Microstructure of Mg-2.5Zn-1Ca: (a) cast sample; (b) after heat-treatment; (c) extruded rod; (d) extruded micro-tube.

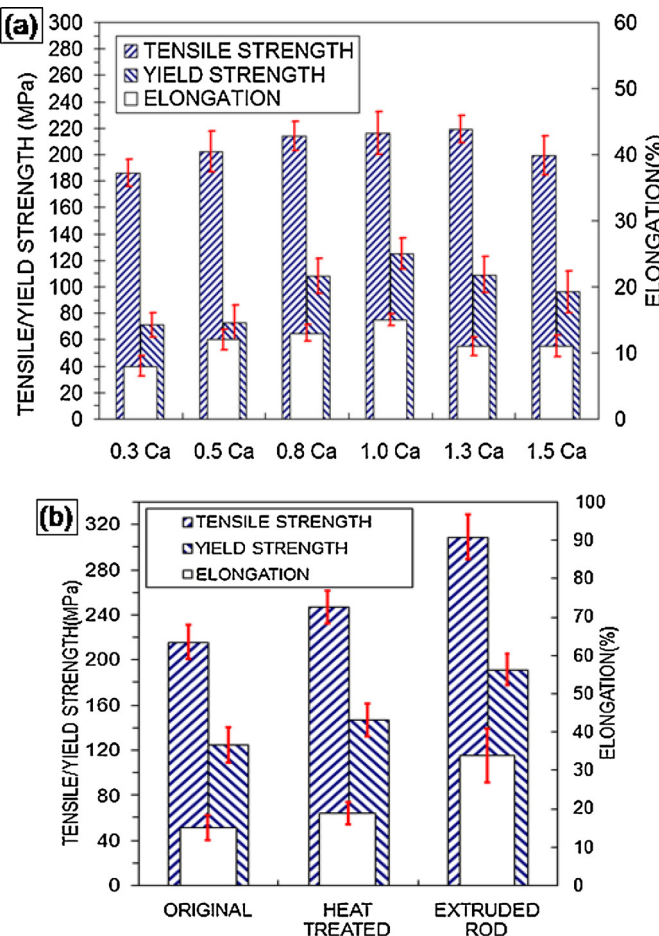
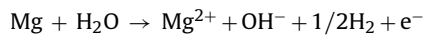


**Fig. 6.** SEM images of the fracture surface morphology: (a) cast sample; (b) after heat-treatment; (c) extruded rod; (d) extruded micro-tube.

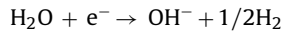
It has been previously reported that the following two factors will have a significant influence on mechanical properties, electrochemical response and corrosion reactivity: (i) changes in the overall grain structure, including grain shape, character of grain boundaries and misorientation, especially reduction in the average grain size; and (ii) redistribution of solute atoms due to second-phase particle break-up and/or re-solutionizing [38,39].

The electrochemical corrosion mechanisms and pH value variation can be explained by the following chemical reaction:

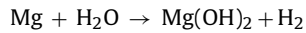
At the anode:



At the cathode:



The possible total reaction is:



For the cast alloy, the sharp increase of pH may be attributed to serious component segregation within the grain as well as the accumulation of non-equilibrium phases in grain boundary. When the pH value is higher than 10.5, created  $\text{Mg}(\text{OH})_2$  film at the surface of the 'anode' became stable to a large extent and its film become compact and protective. It can be seen that the corresponding pH curve are flattened at the later period of test.

For the double extruded alloys, the results reveal that the above-mentioned reaction was yield after fine grain strengthening. On the one hand, the reaction could be accelerated at the beginning of the immersion test. Accordingly, the formation of contact  $\text{Mg}(\text{OH})_2$  film would bring protective effect earlier than in the cast alloy. On the other hand, depending on specific elements, material state and environment combinations, the redistribution and possible resolutionizing of intermetallic particles plays a vital role in the corrosion and passivation processes [40].

It is also reported that increased grain boundary density could either increase or decrease the corrosion rate depending on environment and material factors. Moreover, the influence cannot be

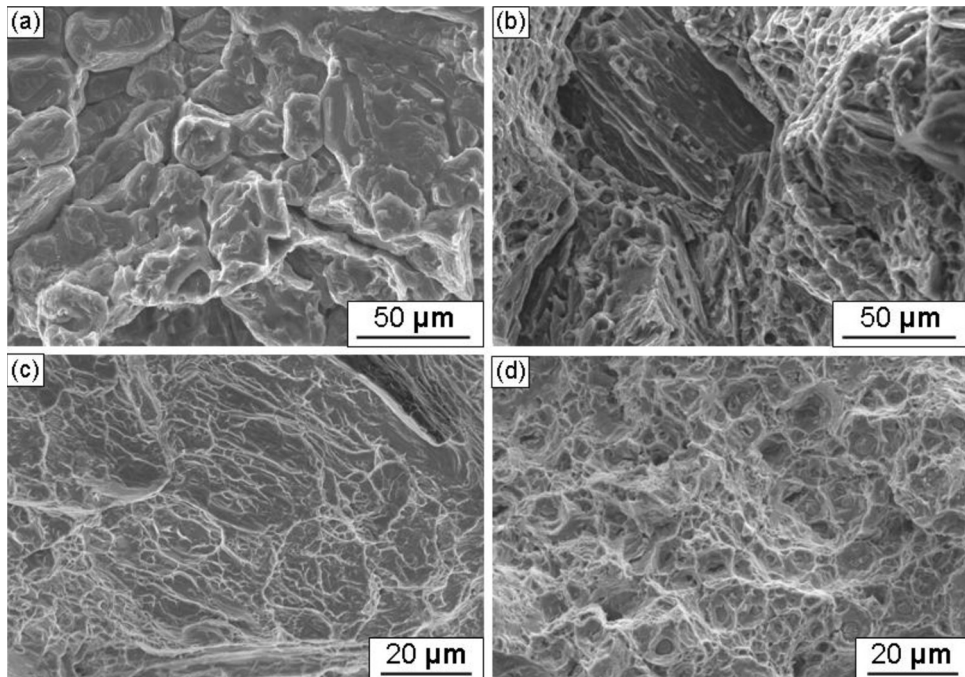


**Fig. 7.** Immersion test results: (a) corrosion rate of different samples as function of immersion time; (b) pH value variation as function of immersion time.

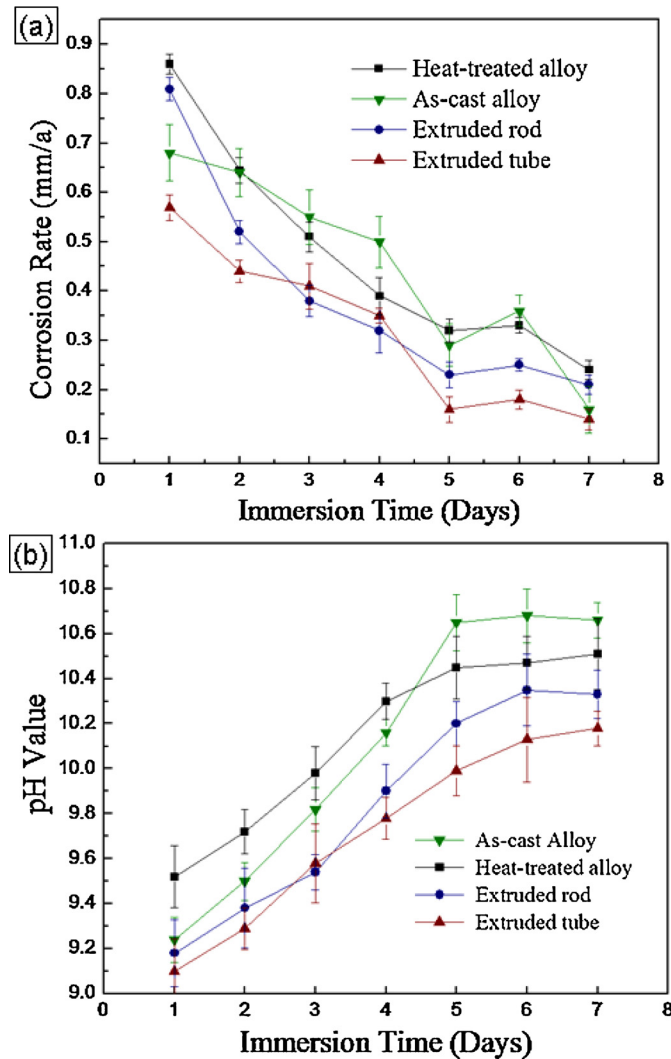


**Fig. 8.** Immersion test results: (a) corrosion rate of different samples as function of immersion time; (b) pH value variation as function of immersion time.

attributed exclusively to grain size because the whole processing simultaneously induces a reorganization of the solute distribution throughout the microstructure. Disordered non-crystalline films have been noted to be more protective than ordered crystalline films by restricting ion movement and increasing the breakdown and repassivation rates [41]. The fine-grained structure of the bulk material produced by the processing mentioned above promotes the formation of a more protective surface film.

The protective film formation attributed to grain refinement could be explained from the perspective of a decreased degree of mismatch between MgO and the underlying Mg matrix. The free volume mismatch between the oxide and the metallic substrate gives rise to tensile stresses in the oxide, thereby increasing its propensity for dissolution [40]. This mismatch in the unit volume element is especially effective in generating tensile stress in oxides on Mg alloys with coarse grain size. A fine-grained microstructure achieved as a result of comprehensive processing procedures induces porosity with the increased grain boundary density, likely providing a means for relieving the tensile stress and thus reducing the propensity of oxide cracking [40]. The film formed on Mg matrix is composed of a thin inner MgO layer covered with Mg(OH)<sub>2</sub>. The cubic MgO may also transform to hexagonal Mg(OH)<sub>2</sub> upon hydration [42–44]. Thus, a protective MgO layer would provide better surface coverage for Mg matrix and inhibit subsequent rupture of

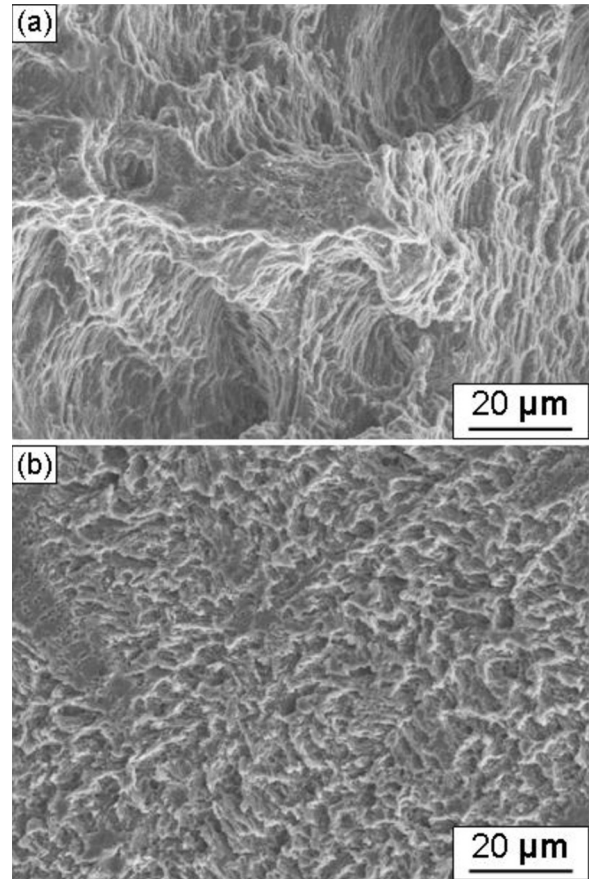


**Fig. 9.** Corrosion morphologies of Mg alloy in Hank's solution for 8 days: (a) cast alloy with heat-treatment; (b) double extruded micro-tube.

the exterior Mg(OH)<sub>2</sub> layer by providing a better matched transition. This would explain the slower corrosion rates observed in the processed samples after fine-grain and solid solution strengthening.

The degradation process of Mg alloy *in vivo* could be viewed as a result of mechanical failure and material corrosion. From the perspective of mechanical properties, hot extrusion may impart a significant influence on the precise deformation of an implant and its corrosion fatigue in special biologically stressed environment. Although hot extrusion cannot eliminate the high corrosion rate of Mg alloy completely, the degradation will be yielded to some extent to match the healing and regenerating processes, in which implants are demanded for maintaining more than 3 months in body.

## 5. Summary and conclusions

- (1) An optimized choice of alloy composition, vacuum melting, heat-treatment, integrated plastic deformation and micro-tube forward extrusion parameters were developed for a comprehensive processing technique to form Mg alloy into micro-tubes for degradable implant stents.
- (2) Compared to the original cast alloy, the overall mechanical properties of extruded micro-tube are significantly improved due to fine-grain strengthening and solid solution strengthening.
- (3) Mg alloy processed by the procedures shows better corrosion resistance. There appears to be a correlation between corrosion resistance and grain size connected with microstructure evolution caused by multiple hot extrusions.

## Acknowledgements

One of the authors (DXL) was supported by the Chinese Scholarship Council. This work was supported in part by the National Nature Science Foundation of China under Grant No. 51365029 and the fundamental research funds of Gansu province for higher education institutions. Marc Meyers and Vincent Sherman would like to acknowledge support by NSF Grant 1006931 and U.C. Research Laboratories Grant 09-LR-06-118456-MEYM.

## References

- [1] E.D. McBride, J. Am. Med. Assoc. 111 (1938) 2464.
- [2] J. Verbrugge, La Press. Med. 23 (1934) 460.
- [3] F. Witte, V. Kaeseb, H. Haferkamp, E. Switzer, A. Meyer-Lindenberg, C.J. Wirtha, H. Windhagena, Biomaterials 26 (2005) 3557.
- [4] B. Heublein, R. Rohde, V. Kaese, M. Niemeyer, W. Hartung, A. Haverich, Heart 89 (2003) 651.
- [5] P. Zartner, R. Cesnjevar, H. Singer, M. Weyand, Catheter. Cardiovasc. Interv. 66 (2005) 590.
- [6] R. Waksman, Catheter. Cardiovasc. Interv. 70 (2007) 407.
- [7] X.N. Gu, Y.F. Zheng, Front. Mater. Sci. China 4 (2010) 111.
- [8] R.S. Stack, R.M. Calif, H.R. Phillips, D.B. Pryor, P.J. Quigley, R.P. Bauman, Am. J. Cardiol. 62 (1988) 3F.
- [9] S.J. Kalita, S. Bose, H.L. Hosick, A. Bandyopadhyay, Mater. Sci. Eng. C 23 (2003) 611.
- [10] R. Erbel, C.D. Mario, J. Bartunek, J. Bonnier, B. de Bruyne, F.R. Eberli, P. Erne, M. Haude, B. Heublein, M. Horrigan, C. Illesley, D. Böse, J. Koolen, T.F. Lüscher, N. Weissman, R. Waksman, Lancet 369 (2007) 1869.
- [11] M. Kannan, R.K. Raman, Biomaterials 29 (2008) 2306.
- [12] N.T. Kirkland, N. Birbilis, M.P. Staiger, Acta Biomater. 8 (2012) 925.
- [13] W.D. Mueller, M. Lucia Nascimento, M.F. Lorenzo de Mele, Acta Biomater. 5 (2010) 1749.
- [14] X.N. Gu, W. Zheng, Y. Cheng, Y.F. Zheng, Acta Biomater. 5 (2009) 2790.
- [15] D.C. Xue, Z.Q. Tan, M.J. Schulz, W.J. Vanooij, J. Sankar, Y. Yun, Z.Y. Dong, Mater. Sci. Eng. C 32 (2012) 1230.
- [16] Y. Wang, M. Wei, J.C. Gao, Mater. Sci. Eng. C 29 (2009) 1311.
- [17] L.P. Xu, F. Pan, G.N. Yu, L. Yang, E.L. Zhang, K. Yang, Biomaterials 30 (2009) 1512.
- [18] H.X. Wang, S.K. Guan, X. Wang, C.X. Ren, L.G. Wang, Acta Biomater. 6 (2010) 1743.
- [19] H.M. Wong, K.W. Yeung, K.O. Lam, V. Tam, P.K. Chu, K.D. Luk, K.M. Cheung, Biomaterials 31 (2010) 2084.
- [20] F. Feyerabend, J. Fischer, J. Holtz, F. Witte, R. Willumeit, H. Drücker, C. Vogt, N. Hort, Acta Biomater. 5 (2010) 1834.
- [21] E.L. Zhang, L. Yang, J.W. Xu, H.Y. Chen, Acta Biomater. 5 (2010) 1756.
- [22] N. Erdmann, N. Angrisani, J. Reifenrath, A. Lucas, F. Thorey, D. Bormann, A. Meyer-Lindenberg, Acta Biomater. 3 (2011) 1421.
- [23] X.N. Gu, Y.F. Zheng, Y. Cheng, S.P. Zhong, T.F. Xi, Biomaterials 30 (2009) 484.
- [24] Y.C. Li, C.E. Wen, D. Mushahary, R. Sravanthi, N. Harishankar, G. Pande, P. Hodgson, Acta Biomater. 8 (2012) 3177.
- [25] L. Choudhary, R.K. Singh Raman, Acta Biomater. 2 (2012) 916.
- [26] P.M. Jardim, G. Solorzano, J.B. Vander Sande, Microsc. Microanal. 8 (2002) 487.
- [27] N. Birbilis, M.K. Cavanaugh, A.D. Sudholz, S.M. Zhu, M.A. Easton, M.A. Gibson, Corros. Sci. 53 (2011) 168.
- [28] S.X. Zhang, X.N. Zhang, C.L. Zhao, J.A. Li, Y. Song, C.Y. Xie, H.R. Tao, Y. Zhang, Y.H. He, Y. Jiang, Y.J. Bian, Acta Biomater. 6 (2010) 626.
- [29] J. Nagels, M. Stokdijk, P.M. Rozing, J. Shoulder Elbow Surg. 12 (2003) 35.
- [30] R.B. Figueiredo, T.G. Langdon, Mater. Sci. Eng. A 501 (2009) 105.
- [31] R.B. Figueiredo, T.G. Langdon, Mater. Sci. Eng. A 503 (2009) 141.
- [32] C.M. Liu, B.F. Li, R. Wang, H.Z. Li, Z.Y. Chen, Chin. J. Nonferr. Metal 20 (2010) 171.
- [33] W. Zhai, W.L. Wang, D.L. Geng, B. Wei, Acta Mater. 60 (2012) 6518.
- [34] D.H. Stjohn, M. Qian, M.A. Easton, P. Cao, Z. Hildebrand, Mater. Mater. Trans. 36A (2005) 1669.
- [35] M.R. Barnett, Z. Keshavarz, A.G. Beer, D. Atwell, Acta Mater. 52 (2004) 5093.
- [36] G. Nussbaum, P. Sainfort, G. Regazzoni, H. Gjestland, Scr. Metall. 23 (1989) 1079.
- [37] M. Mabuchi, K. Ameyama, H. Iwasaki, K. Higashi, Acta Mater. 7 (1999) 2047.
- [38] R.Z. Valiev, T.G. Langdon, Prog. Mater. Sci. 51 (2006) 881.
- [39] M. Murayama, Z. Horita, K. Hono, Acta Mater. 49 (2001) 21.
- [40] D. Orlov, K.D. Ralston, N. Birbilis, Y. Estrin, Acta Biomater. 59 (2011) 6176.
- [41] G.L. Makar, J. Kruger, Int. Mater. Rev. 38 (1993) 138.
- [42] H.B. Yao, Y. Li, A.T.S. Wee, Appl. Surf. Sci. 158 (2000) 112.
- [43] M. Santamaría, F. Di Quarto, S. Zanna, P. Marcus, Electrochim. Acta 53 (2007) 1314.
- [44] M. Liu, S. Zanna, H. Ardelean, I. Frateur, P. Schmutz, Corros. Sci. 51 (2009) 1115.